Electronic Supporting Information

A temperature-adjustable in situ infrared diffuse reflectance spectroscopy system for catalysts

*Weifeng Huang ‡[ab], Tao Chen‡[a], Jun Luo[b], Geer Su[c], and Hang Wei *[a]*

[a] College of Chemistry and Chemical Engineering, Inner Mongolia Engineering and Technology Research Center for Catalytic Conversion and Utilization of Carbon Resource Molecules, Inner Mongolia University, Hohhot 010021, PR China

[b] College of Chemistry and Chemical Engineering, Qiannan Normal University for Nationalities, Duyun 116023, China

[c] School of Energy Science and Engineering, Nanjing University of Technology, Nanjing 211816, China

* Corresponding Authors.

E-mail addresses: hwf@pku.edu.cn (H. Wei), weihang@imu.edu.cn (H. Wei).

‡ W. Huang and T. Chen contributed equally to this work.

Experimental Section

Preparation of CNT support: The MWCNTs were oxidized by refluxing at 75℃ in concentrated nitric acid for 12 h to introduce carboxyl and hydroxyl groups on the ends and the outer wall of MWCNTs. In this communication, MWCNTs oxidized by concentrated nitric acid were denoted as CNT.

Preparation of CeO_2/CNT support: 1.0 g of $Ce(NO_3)_3$•$6H_2O$ solid and 0.396 g of CNT were dispersed in 100 mL water, and stir for 1.0 h. After the mixture was sonicated, 12.9 mL of dilute ammonia was added to the mixed solution under stirring for 4 h. The precipitate was separated by centrifugation, washed by deionized water and ethyl alcohol for three times respectively, and then calcined at 60℃ under N_2 at 400°C for 4 h. Then the CeO_2/CNT product with the mass ratio of CeO_2 to CNT of 1:1 was obtained.

Preparation of Pt/CNT, PtSb/CNT, Pt/CeO_2/CNT, and PtSb/CeO_2/CNT: 80 mg CNT and 20 mL ethylene glycol were added to 40 ml water. Afterwards, the mixture was ultrasonicated and stirred, and 5.3 mL $HPtCl_6 \cdot 6H_2O$ aqueous solution (10 mg/ml) was added under stirring for 30 min, and refluxed under160°C oil bath for 4 h. Finally, the precipitate was collected and washed by deionized water and pure ethanol for several times and then dried at 60℃ under vacuum to obtain the Pt/CNT catalyst.

The method of synthesizing Pt/CeO_2/CNT catalyst was exactly the same as the above method, the only difference is that 80 mg CNT is replaced by 90 mg CeO_2/CNT.

The method of synthesizing PtSb/CNT catalyst was exactly the same as the synthesizing Pt/CNT method, the only difference is that 5.3 mL $HPtCl_6 \cdot 6H_2O$ aqueous

solution (10 mg/ml) and 206 μL $SbCl_3$ (22.8 mg/ml) were added into the reaction system at the same time.

The method of synthesizing PtSb/ CeO_2/CNT catalyst was exactly the same as the synthesizing PtSb/CNT method, the only difference is that 80 mg CNT is replaced by 90 mg CeO_2/CNT.

Characterizations: Powder X-Ray diffraction (XRD) patterns were collected on a Bruker D8 Advance diffractometer using Cu Kα irradiation (λ=1.5406 Å). The composition and morphology of the nanocomposite were characterized by transmission electron microscope (TEM, TECNAI-F20). Temperature-programmed desorption (TPD) experiments were conducted using TP-5000 equipment. Inductively coupled plasma atomic emission spectrometry (ICP−AES) was performed on an Agilent 700 instrument.

In-situ **FTIR:** In order to authentically understand the intrinsic adsorption and desorption capabilities of these catalysts, we designed a standard procedure. Initially, the synthesized samples are uniformly subjected to vacuum and low-temperature treatment to preserve the real state of the catalysts from the completion of synthesis to their introduction into the production process. Subsequently, the samples are gradually heated under vacuum conditions to understand how temperature affects the material's adsorption and desorption capacity during this process.

In this study, the infrared spectrometer used is the DEEP-FTIR-2 model designed and produced by Beijing Science Star Technology Co., Ltd. An MCT detector is employed as the signal collector, and the optical path adjustment mechanism and in-

situ cell constitute the in-situ system used in this work. The specific experimental procedure involves placing a KBr powder sample in our in-situ cell, which is then inserted into the optical path adjustment mechanism. After vacuuming the entire setup, an infrared background test is conducted. Following the background test, our research sample is placed in the in-situ cell following the same procedure and vacuumed again. Then, using a temperature control system, the temperature of the sample stage is rapidly cooled to -180°C, and subsequently heated rapidly at a rate of 8°C/min up to 300°C. During this heating process, infrared signals are synchronously collected to perform temperature dependency tests on the samples.

Catalytic oxidation of glycerol: Glycerol oxidation was carried out in a three-neck flask (100 mL) containing 10 mL glycerol solution (0.1 mol/L) and 5 mg catalyst. The reactor was sealed and placed in a pretreated oil bath, which was maintained at the required temperature for a given time under vigorous stirring with a magnetic stirrer (IKA). Once the temperature was stabilized at the specified reaction temperature (30, 40, 50˚C), O_2 (99.9%) was introduced to the reactor at a rate of 150 mL/min via a mass flow controller. At the end of the predetermined reaction time, 1mL of solution was taken out from the flask, and the catalyst was removed by filtration and the aqueous solution was analyzed using an Agilent 1260 high performance liquid chromatograph (HPLC). The HPLC was equipped with UV-detector (210 nm) and refractive index detector (RID) using a Zorbax SAX column (4.6mm × 250 mm, Agilent) operating at 308 K. The eluent was an acetonitrile aqueous solution of H_3PO_4 (0.001 g/mL) operating at 1.0 mL/min. By injecting the standard samples solution, calibration curves

and the retention time of each product were obtained. Meanwhile, the concentrations of different products were determined with the obtained calibration curves. All standard samples were purchased from Alfa, SIGMA and TCI.

Discussion Section

Detailed elucidation of Figure 3: While Figure 2 effectively illustrates the varying sensitivities of different Pt-based catalysts to temperature changes, it is important to note that the catalytic reactions in this system predominantly occur within a temperature range of 100℃. To gain a more refined understanding of the catalysts' temperature dependence within a narrower scope, we have adjusted the temperature range for analysis to -30 to 80℃. This adjustment is aimed at discerning the subtle differences between the catalysts' responses to temperature variations more clearly. To enhance the detection of these nuances, we employed the synchronous spectrum method, known for its superior capability in recognizing minor differences. Figure 3, as a result, delineates the relationship between varying catalysts and temperature changes, providing a detailed comparison.

The synchronous correlation spectrum (Figure 3a) reveals distinct characteristics for different catalysts. Notably, Pt/CNT, Pt/CeO_2/CNT, and PtSb/CeO_2/CNT each exhibit auto-peaks of varying intensities around the wavenumbers 1550 cm^{-1} and 1650 cm^{-1}. In contrast, PtSb does not display any significant auto-peaks across the entire analyzed range. This observation suggests that the incorporation of Sb and CeO_2 into the Pt catalysts alters their thermal response, highlighting the intricate relationship between catalyst composition and temperature sensitivity. Such insights are crucial for

understanding the catalysts' behavior under specific operational conditions, thereby informing the optimization of catalytic performance in practical applications.

As elucidated in Figure 2, the wavenumbers 1550 and 1650 cm^{-1} represent critical points for adsorbents within our system, with their temperature-dependent variations significantly impacting catalytic efficiency. Analysis of Figure 3a reveals that the auto-peak value for $Pt/CeO_2/CNT$ at 1650 cm^{-1} is positive, suggesting that the absorption infrared peak intensifies as temperature increases. This implies a heightened adsorption capacity for oxygen-containing substances at elevated temperatures for $Pt/CeO_2/CNT$. Conversely, the auto-peaks for Pt/CNT and $PtSb/CeO_2/CNT$ are negative, indicating a reduction in infrared absorption peak intensity with decreasing temperature. This trend suggests an increasing desorption capability for oxygen-containing materials as temperatures lower. The absence of noticeable auto-peaks signifies stable infrared peaks, indicating negligible changes in adsorption and desorption capabilities. This nuanced understanding of how different catalysts interact with temperature underscores the complex interplay between adsorption/desorption dynamics and catalytic performance, offering valuable insights into optimizing catalyst design for specific reactions.

The variations in the intensity of the absorption infrared peaks, as discussed, not only reveal differences in adsorption and desorption dynamics but also correlate directly with the catalytic reaction capabilities of the catalysts under study. This correlation is strikingly consistent with the observed hierarchy of catalytic efficiency in subsequent reactions ($Pt/CeO_2/CNT$ > Pt/CNT > $PtSb/CeO_2/CNT$ > PtSb/CNT). Figure 3b

showcases the uncorrelated spectra, where the observed trends in the cross peaks, such as around 1650 cm^{-1}, correspond with the patterns identified in the auto-peaks of the synchronous spectrum. This congruence suggests a consistent relationship between the adsorption and desorption capabilities of the COO^- functional group and temperature variations. Such findings highlight the nuanced interplay between spectral changes and catalytic activity, further validating the predictive value of infrared spectral analysis in understanding catalyst performance dynamics.

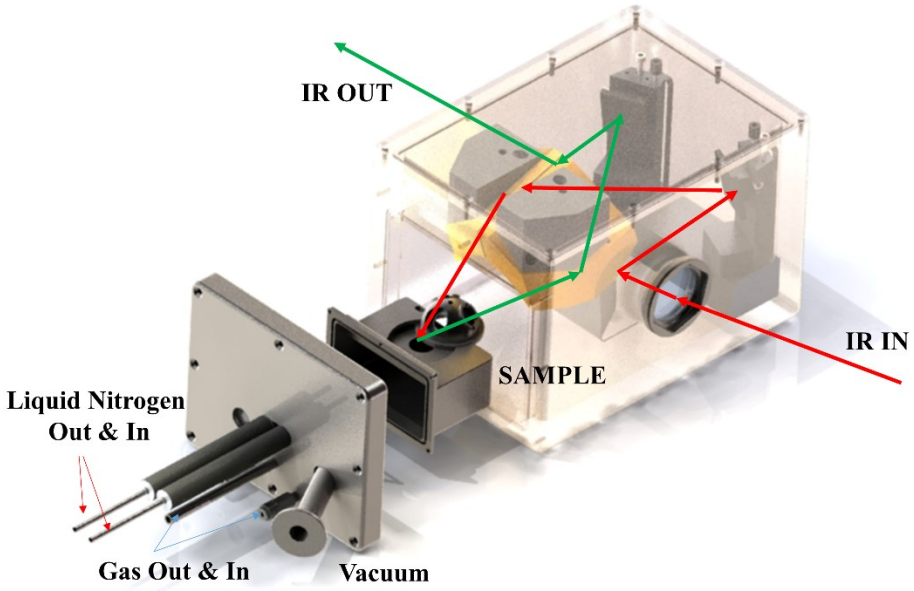

Figure S1 schematic diagram of the vacuum box with light path adjustment and gas intake.

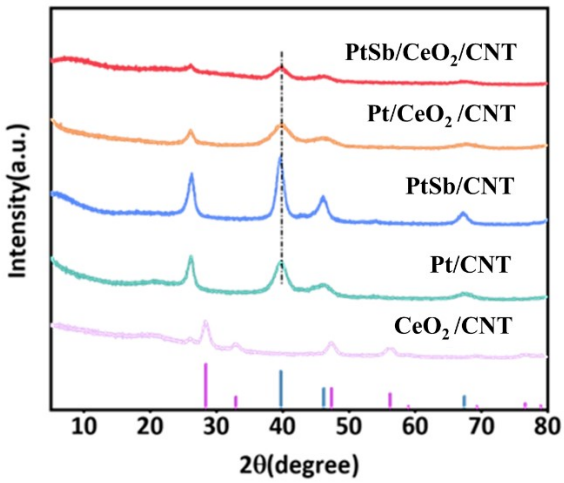

Figure S2 The XRD patterns of as-prepared Pt/CNT, PtSb/CNT, Pt/CeO_2/CNT, and PtSb/CeO_2/CNT.

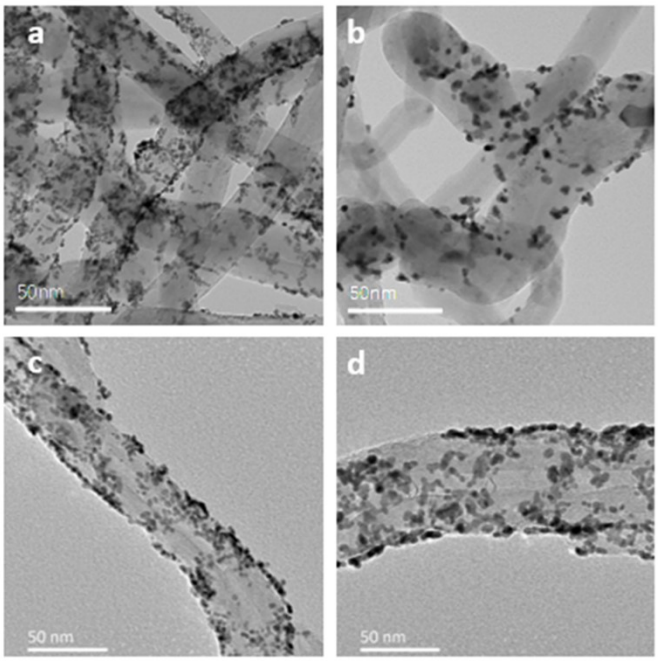

Figure S3 The TEM images of as-prepared (a) Pt/CNT, (b) PtSb/CNT, (c) Pt/CeO_2/CNT, and (d) PtSb/CeO_2/CNT.

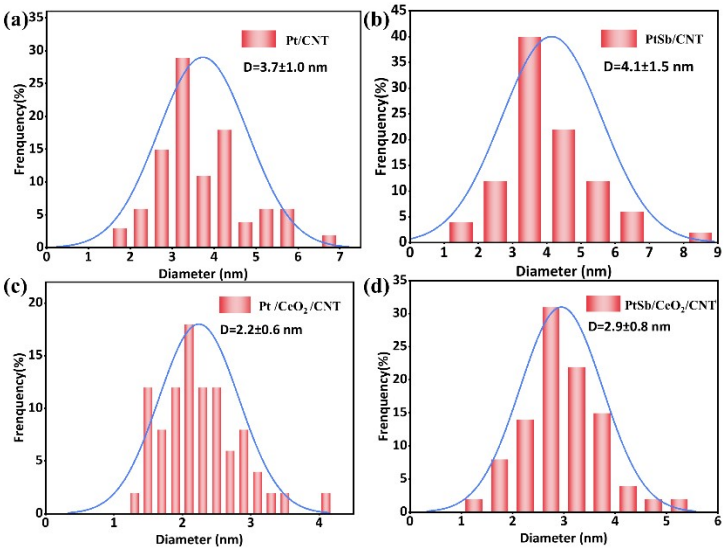

Figure S4 The size distribution of Pt nanoparticles in (a) Pt/CNT, (b) PtSb/CNT, (c) $Pt/CeO_2/CNT$ and (d) $PtSb/CeO_2/CNT$.

Table S1 The size of Pt nanoparticles calculated from Scherre formula in the four catalysts.

Sample	**Diameter**
Pt/CNT	4.2
PtSb/CNT	4.7
$Pt/CeO_2/CNT$	3.3
$PtSb/CeO_2/CNT$	4.0

Table S2 ICP data of the four catalysts.

Sample	**Pt%**
Pt/CNT	18.12
PtSb/CNT	17.67
$Pt/CeO_2/CNT$	18.36
$PtSb/CeO_2/CNT$	17.97

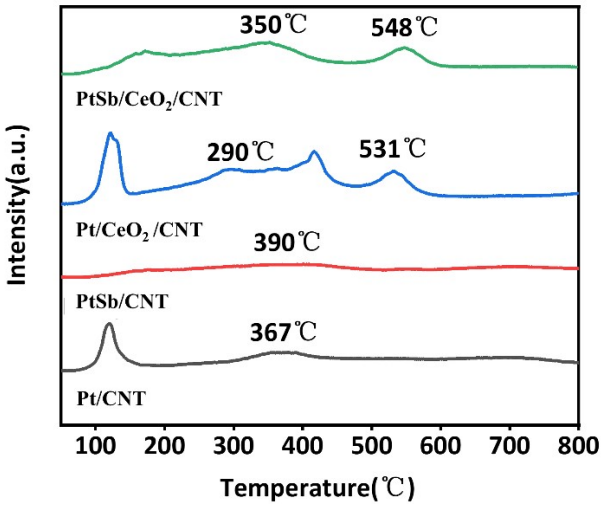

Figure S5 The O_2-TPD profiles of as-prepared Pt/CNT, PtSb/CNT, Pt/CeO_2/CNT, and PtSb/CeO_2/CNT.